



Fetal development of subcutaneous white adipose tissue is dependent on Zfp423

Mengle Shao, Chelsea Hepler, Lavanya Vishvanath, Karen A. MacPherson, Napoleon C. Busbuso, Rana K. Gupta*

ABSTRACT

Objective: *Zfp423* is a multi zinc-finger transcription factor expressed in preadipocytes and mature adipocytes *in vivo*. Our recent work has revealed a critical role for *Zfp423* in maintaining the fate of white adipocytes in adult mice through suppression of the beige cell thermogenic gene program; loss of *Zfp423* in mature adipocytes of adult mice results in a white-to-beige phenotypic switch. However, the exact requirements of *Zfp423* in the fetal stages of early adipose development *in vivo* have not been clarified.

Method: Here, we utilize two models that confer adipose-specific *Zfp423* inactivation during fetal adipose development (*Adiponectin*-Cre; *Zfp423*^{loxP/loxP} and *Adiponectin*-rtTA; TRE-Cre; *Zfp423*^{loxP/loxP}). We assess the impact of fetal adipose *Zfp423* deletion on the initial formation of adipose tissue and evaluate the metabolic consequences of challenging these animals with high-fat diet feeding.

Results: Deletion of *Zfp423* during fetal adipose development results in a different phenotype than is observed when deleting *Zfp423* in adipocytes of adult mice. Inactivation of *Zfp423* during fetal adipose development results in arrested differentiation, specifically of inguinal white adipocytes, rather than a white-to-beige phenotypic switch that occurs when *Zfp423* is inactivated in adult mice. This is likely explained by the observation that *adiponectin* driven Cre expression is active at an earlier stage of the adipocyte life cycle during fetal subcutaneous adipose development than in adult mice. Upon high-fat diet feeding, obese adipose *Zfp423*-deficient animals undergo a pathological adipose tissue expansion, associated with ectopic lipid deposition and systemic insulin resistance.

Conclusions: Our results reveal that *Zfp423* is essential for the terminal differentiation of subcutaneous white adipocytes during fetal adipose tissue development. Moreover, our data highlight the striking adverse effects of pathological subcutaneous adipose tissue remodeling on visceral adipose function and systemic nutrient homeostasis in obesity. Importantly, these data reveal the distinct phenotypes that can occur when *adiponectin* driven transgenes are activated in fetal vs. adult adipose tissue.

© 2016 The Authors. Published by Elsevier GmbH. This is an open access article under the CC BY-NC-ND license (<http://creativecommons.org/licenses/by-nc-nd/4.0/>).

Keywords Adipogenesis; Zfp423; Pparg; Subcutaneous adipocytes; Preadipocytes; Obesity; Insulin resistance

1. INTRODUCTION

White adipocytes are the primary cell type in mammals for safe energy storage in the form of triglyceride. These cells are characterized by their large single (unilocular) lipid-droplet appearance and the presence of the enzymatic machinery to synthesize triglyceride for storage in times of energy surplus. White adipocytes also produce hormones and circulating cytokines (termed adipokines) that regulate food intake and nutrient homeostasis [1]. Brown and beige adipocytes are heat-producing, or “thermogenic,” adipocytes that are characterized by their abundance of mitochondria and ability to burn stored energy to produce heat [2,3]. This thermogenic capacity is mostly mediated by uncoupling protein 1 (Ucp1). Ucp1 is a transport protein that sits within the inner mitochondrial membrane and facilitates a proton leak [4].

The importance of white adipose tissue is highlighted by two seemingly disparate conditions. An absence of adipose tissue, or “lipodystrophy,” results in the loss of protective adipokines (e.g.

adiponectin and leptin) and ectopic lipid accumulation in non-adipose tissues such as the liver, muscle, and pancreas. The latter is deleterious to nutrient homeostasis, as excessive accumulation of lipid species can trigger insulin resistance and cardiovascular disease [5]. Increased adiposity, as seen in the condition of obesity, also confers significant risk for developing the same chronic disorders, including insulin resistance, diabetes mellitus, cardiovascular disease, and cancer. However, a significant portion of obese individuals appears relatively resistant to acquiring metabolic syndrome, at least for a period of time [6–8]. This suggests that additional factors, outside of increased adiposity *per se*, determine metabolic health in obesity. One clear predictor of metabolic disease in the setting of obesity is the cellularity of adipose depots [9,10]. Adipose tissue expansion in obesity, in principle, can occur through increased lipid-loading into existing adipocytes, leading to increased cell size, or “adipocyte hypertrophy.” Adipocyte hypertrophy is characteristic of adipose tissue in obese individuals with metabolic syndrome. The prevailing theory is that engorged fat cells outstrip their vascular supply, leading to local

Touchstone Diabetes Center, Department of Internal Medicine, University of Texas Southwestern Medical Center, Dallas, TX 75390, USA

*Corresponding author. Touchstone Diabetes Center, Department of Internal Medicine, UT Southwestern Medical Center, 5323 Harry Hines Blvd., K5.240, Dallas, TX 75390-8549, USA. E-mail: Rana.Gupta@UTSouthwestern.edu (R.K. Gupta).

Received October 26, 2016 • Revision received November 11, 2016 • Accepted November 15, 2016 • Available online 21 November 2016

<http://dx.doi.org/10.1016/j.molmet.2016.11.009>

hypoxia, fibrosis, adipocyte dysfunction, and cell death [11–16]. Similar to what is observed in lipodystrophy, excess lipid is deposited in peripheral non-adipose tissues that are incapable of safely storing excessive amounts of triglyceride.

Increases in fat cell number, or “adipocyte hyperplasia,” can also occur in obese individuals, resulting in the accumulation of more numerous adipocytes at the expense of large hypertrophic adipocytes. “Healthy-obese” individuals, in comparison to BMI-matched individuals with metabolic syndrome, often exhibit an adipose phenotype characterized by smaller and more numerous adipocytes. This strongly correlates with low inflammation, fibrosis, and preservation of circulating levels of the insulin-sensitizing hormone adiponectin [17–19]. The storage of triglyceride over numerous adipocytes is believed to help limit the loss of adipocyte function. These observations imply that adipocyte recruitment is protective in obesity and that a pathological hypertrophic adipose expansion in obesity effectively creates a “partial lipodystrophic” phenotype.

Clinical studies also point to the location of excess adipose accumulation as one of the best predictors of metabolic health. Individuals who preferentially store excess adiposity in the visceral compartment are at a greater risk than those who accumulate adipose tissue in the subcutaneous region [20]. In fact, subcutaneous adipose tissue appears protective against insulin resistance [21]. Some engineered mouse models preferentially accumulate subcutaneous WAT and exhibit a metabolically healthy obese phenotype [22,23]. Thus, the preservation of functional subcutaneous WAT is widely believed to be critical for the maintenance of whole body metabolic homeostasis. However, the precise requirements of functional subcutaneous WAT *in vivo* have not been directly assessed, in large part because genetic tools to manipulate WAT in a depot-selective manner have been lacking.

The main transcriptional machinery that governs adipogenesis has been carefully elucidated, largely using cell culture models [24–26]. The nuclear hormone receptor, Ppar γ , represents the key regulator of adipocyte differentiation [27]. We have previously identified the multi-C2H2 zinc-finger transcription factor, Zfp423, as a regulator of multiple stages of the adipocyte life cycle. Zfp423 expression identifies committed peri-endothelial preadipocytes that reside in the adipose tissue vasculature and contribute to white adipocyte hyperplasia associated with high-fat diet feeding [28,29]. In cells, Zfp423 regulates preadipocyte commitment and differentiation, at least in part through regulation of preadipocyte levels of Ppar γ [30]. Zfp423 is also expressed in fully differentiated adipocytes; however, expression is higher in white adipocytes as compared to brown adipocytes. In mature white adipocytes, Zfp423 functions to suppress the thermogenic gene program, thereby maintaining the white adipocyte identity of these cells [31].

Genetic evidence supporting a critical role for Zfp423 in maintaining the white adipose lineage comes from our recent study in which we utilized a doxycycline-inducible system for Cre-mediated inactivation of Zfp423 in adult adipocytes (Adiponectin-rtTA; TRE-Cre; Zfp423^{loxP/loxP}; “Zfp423-iAKO” mice) [31]. Inducible adipocyte-specific inactivation of Zfp423 in adult mice leads to a robust conversion of mature white adipocytes into thermogenic, beige-like cells. These data revealed that Zfp423 is required in differentiated white adipocytes to suppress the thermogenic gene program and maintain the white adipocyte identity. However, clear genetic evidence supporting a role for Zfp423 in the initial formation of adipocytes has been lacking. Germline inactivation of Zfp423 (Zfp423^{-/-}) in mice results in malformation of the central nervous system and perinatal death [32–34]. Analysis of Zfp423^{-/-} embryos (embryonic day 18.5) revealed a severe defect in interscapular brown adipose tissue (BAT) formation

and a reduction in the numbers of nascent subdermal white adipocytes present at this stage [30]. However, the importance of Zfp423 to white adipose depot development could not be fully clarified given the other confounding phenotypes in this model.

In this study, we reveal that the loss of adipose Zfp423 during fetal WAT development leads to arrested terminal differentiation of inguinal white adipocytes by the time of birth. Upon high-fat diet feeding as adults, Zfp423-deficient animals become obese but exhibit a metabolic phenotype similar to that of partial lipodystrophy, characterized by pathological inguinal WAT expansion, hepatic steatosis, and systemic insulin resistance. This developmental defect can be rescued by administering the Ppar γ ligand, rosiglitazone, specifically during the fetal and early postnatal period. All together, these data define Zfp423 as a critical regulator of adipose development and illustrate the systemic metabolic consequences of pathological subcutaneous adipose tissue expansion in obesity.

2. MATERIALS AND METHODS

2.1. Animals

The *Pdgfra-Cre* (stock# 013148), *Adiponectin-Cre* (stock# 010803), and *Rosa26R^{loxP-stop-loxP-tdtomato}* transgenic strains were from Jackson lab. Zfp423^{loxP/loxP} mice were a generous gift from Dr. S. Warming (Genentech, Inc.) [34]. Adiponectin^{rtTA} and TRE-Cre transgenic mice have been described previously [35]. Mice were maintained with a 12-hour light/dark cycle and free access to food and water. All animal experiments were performed according to procedures approved by the UTSW Institutional Animal Care and Use Committee.

2.2. Histological analysis

Tissues were dissected and fixed in 4% paraformaldehyde overnight. Paraffin processing, embedding, sectioning, and standard hematoxylin and eosin (H&E) staining were performed at the Molecular Pathology Core Facility at UTSW. Bright-field and fluorescent images were acquired using Keyence BZ-X710 microscope. Adipocyte size analysis was conducted following published protocols with minor modifications [36]. Keyence BZ-X Analyzer software was used for analysis based on bright-field images of H&E-stained paraffin sections. >300 adipocytes were quantified in each individual animal.

2.3. Indirect immunofluorescence

The following antibodies and concentrations were used: guinea pig anti-perilipin 1:1500 (Fitzgerald 20R-PP004); rabbit anti-F4/80 1:500 (Santa Cruz M-300); donkey anti-rabbit Alexa 647 1:200 (Invitrogen); and goat anti-guinea pig Alexa 488 1:200 (Invitrogen). Paraffin sections were dewaxed and hydrated in Xylene and 100%–95%–80%–70%–50% Ethanol and ddH₂O. Slides were placed in chambers containing 1 × R-Buffer A pH 6.0 solution and antigen retrieval was done using Antigen Retriever 2100 (Electron Microscopy Sciences) for 2 h. Following PBS wash for 5 min, Fx Signal Enhancer (Invitrogen) was added to the slides for 30 min at room temperature. Slides were then blocked for 30 min in PBS containing 10% normal goat serum at room temperature. Primary antibodies were then diluted in PBS containing 10% normal goat serum and added to paraffin sections overnight at 4 °C. Following overnight incubation, slides were washed in PBS and incubated with secondary antibodies diluted in PBS containing 10% normal goat serum for 2 h at room temperature. Washed slides were mounted with Prolong Anti-Fade mounting medium containing DAPI (Invitrogen) before images were acquired for analysis.

2.4. *In vivo* insulin stimulation

After 6-hour fasting, animals were anesthetized and injected with insulin (1 U/kg for chow-fed mice; 2 U/kg for HFD-fed mice) through the portal vein. 5 min after the injection, iWAT, gWAT, and liver were quickly snap-frozen for subsequent analysis. Samples harvested before insulin injection were used as untreated controls.

2.5. Immunoblotting and antibodies

Protein extracts from cells or tissues were prepared by homogenization in RIPA lysis buffer (Santa Cruz). Protein extracts were separated by SDS-polyacrylamide gel electrophoresis (SDS-PAGE) and transferred onto PVDF membrane (Millipore). After incubation with the indicated primary antibodies at 4 °C overnight, the blots were incubated with IR Dye-coupled secondary antibodies (LI-COR) and visualized by the LI-COR Odyssey infrared imaging system. The anti-pSer473-Akt (#9271) and anti-Akt (#9272) antibodies were from Cell Signaling. The anti-Adiponectin antibody was from Dr. P.E. Scherer (UTSW).

2.6. Isolation of adipose stromal vascular fraction (SVF) and *in vitro* differentiation

White fat tissues dissected from mice (4–5 weeks of age) were washed in PBS, minced thoroughly, and digested in vacuum filtered digestion buffer (100 mM Hepes PH 7.4, 120 mM NaCl, 50 mM KCl, 5 mM glucose, 1 mM CaCl₂, 1.5% bovine serum albumin, and 1 mg ml⁻¹ collagenase D) for 2 h at 37 °C with shaking. Digested tissues were then filtered through 100 μm cell strainers to remove undigested tissues. The flow-through was centrifuged for 5 min at 600 g to pellet the stromal vascular cells. The floating adipocyte layer was discarded and the stromal vascular cells were re-suspended in growth media containing DMEM/F12 (Invitrogen) plus 10% FBS. For *in vitro* differentiation, SVF cells isolated by collagenase digestion were plated onto collagen-coated dishes and cultured in 10% CO₂ at 37 °C to reach confluency. Confluent cultures were stimulated with adipogenic cocktail (growth media supplemented with 5 μg ml⁻¹ insulin, 1 μM dexamethasone, 0.5 mM isobutylmethylxanthine, and 1 μM rosiglitazone when indicated) for 48 h. Subsequently, cells were maintained in growth media supplemented with 5 μg ml⁻¹ insulin until harvest.

2.7. Flow cytometry analysis

Stromal vascular fraction cells from either inguinal or gonadal WAT depots were first incubated on ice for 20 min in 2% FBS/PBS containing anti-mouse CD16/CD32 Fc Block (clone 2.4G2) (1:200). Cells were then incubated with primary antibody (anti-CD31 clone 390 1:200, anti-CD45 clone 30-F11 1:200, anti-Pdgfrα clone 16A1 1:100), incubated rotating at 4 °C for 30 min, washed three times with 2% FBS/PBS, and then analyzed using a FACSCalibur™ flow cytometer at UT Southwestern Medical Center Flow Cytometry Core Facility. All antibodies were obtained commercially from BioLegend (San Diego, CA USA).

2.8. *In vitro* and *ex vivo* lipolysis assay

In vitro lipolysis was performed on SVF-derived adipocytes at day 8 after differentiation. For *ex vivo* lipolysis assay, inguinal or gonadal fat pads were surgically removed from Zfp423-AKO mice or control littermates and diced into ~100 mg pieces. Differentiated cells or diced fat pads were then washed with PBS and pre-incubated in 5% CO₂ at 37 °C for 1 h in DMEM plus 2% fatty acid free bovine serum albumin (BSA). After the pre-incubation, cells or diced fat pads were incubated in KRHB buffer (Sigma) plus 2% fatty acid free BSA with the presence of vehicle or 10 μg/ml CL316243 (Sigma) in 5% CO₂ at 37 °C for 2 h.

Free glycerol content in the medium was measured using Free Glycerol Determination Kit (Sigma). Glycerol release from each sample was normalized to the total protein content.

2.9. Oil Red O staining

In vitro differentiated cells were fixed in 10% formalin for 10 min at room temperature. Following fixation, the cells were washed with deionized water twice and incubated in 60% isopropanol for 5 min. Then the cells were completely air dried at room temperature before Oil Red O working solution (2 g l⁻¹ Oil Red O in 60% isopropanol) was added. After incubation at room temperature for 10 min, the Oil Red O solution was removed and the cells were washed with deionized water for 4 times before the images were acquired for analysis.

2.10. Gene expression analysis

Total RNA from tissue or cells was extracted and purified using the TRIzol reagent (Invitrogen) and the RNeasy Mini Kit (Qiagen). cDNA was synthesized with M-MLV reverse transcriptase (Invitrogen) and random hexamer primers (Invitrogen). Relative expression of mRNAs was determined by quantitative PCR using SYBR Green PCR system (Applied Biosystems) and values were normalized to Rps18 levels using the ΔΔ–Ct method. All primer sequences used in the study are provided in [Supplementary Table 1](#).

2.11. Glucose and insulin tolerance test

For glucose tolerance tests (GTT), mice were injected i.p. with glucose (Sigma) at the dosage of 1 g per kg body weight after an overnight fast. For insulin tolerance test (ITT), mice were injected i.p. with 0.75 U human insulin (Eli Lilly) per kg body weight after a fast of 6 h. Blood was collected by venous bleeding from the tail vein at 0, 15, 30, 60, 90, and 120 min post injection. Glucose concentrations were measured using Bayer Contour glucometers.

2.12. Statistical analysis

All data are presented as the mean ± s.e.m. Statistical analysis was performed by unpaired two-tailed Student's t-test or two-way ANOVA analysis with Bonferroni's post-test using Microsoft Excel or Graph Pad Prism 7.0. p values < 0.05 were considered to be statistically significant. No statistical methods were used to predict sample sizes. No randomization or blinding was performed to allocate the samples.

3. RESULTS

3.1. Inactivation of Zfp423 in the Pdgfrα lineage leads to growth defects including arrested development of adipose tissue

Recent insight into the identity and molecular characteristics of adipose precursor populations has begun to inform strategies to target the adipose lineage at early stages of tissue development. Expression of platelet-derived growth factor receptor α-chain (Pdgfrα) identifies a pool of cells within the adipose tissue stroma that contains adipose precursors. Adipose precursors and all adipocytes in the major adipose depots appear to descend from cells with a history of Pdgfrα expression [37]. Despite the widespread expression of endogenous Pdgfrα in mesenchymal populations throughout the mouse, it is reported that one strain of the Pdgfrα-Cre mice efficiently and specifically targets the adipose lineage and can be used for gene ablation at the level of adipose progenitors [37].

Therefore, in order to investigate the role of Zfp423 at the earliest stages of adipogenesis *in vivo*, we developed a mouse strain in which Zfp423 is inactivated specifically in the Pdgfrα-lineage (Pdgfrα^{Lin}) by crossing Pdgfrα-Cre transgenic mice with mice carrying conditional

(loxP-flanked) *Zfp423* alleles (*Pdgfra*-Cre; *Zfp423*^{loxP/loxP} animals, denoted as "*Pdgfra*^{Lin}-*Zfp423*-KO" mice). The *Pdgfra*^{Lin}-*Zfp423*-KO mice were born in the expected Mendelian ratio; however, knockout mice were noticeably smaller in size (Supplementary Figure 1a) and most were not able to survive beyond 4–5 weeks of age. A significant reduction in white adipose depot mass was observed in *Zfp423*-deficient mice compared to control littermates (Supplementary Figure 1b). mRNA levels of adipocyte-selective genes in both inguinal and gonadal WAT were significantly lower in knockout animals as compared to controls (Supplementary Figures 1c and d). These data are consistent with the hypothesis that *Zfp423* is required for the formation of white adipose tissue. However, the striking growth defects in the animals suggest that Cre-mediated recombination of *Zfp423* occurs outside the adipose lineage, thus confounding any further analysis with this model.

3.2. Inguinal adipose tissue development is impaired in *Adiponectin*-Cre; *Zfp423*^{loxP/loxP} mice

Hong et al. recently identified a population of proliferating *Pdgfra*⁺ preadipocytes that emerge in the inguinal WAT depot at E16.5 of development [38]. Interestingly, by E18.5, these cells express adipose progenitor markers (e.g. CD34, CD29, CD24) but also express perilipin and adiponectin; the latter two genes are largely restricted to mature adipocytes after birth. In support of this observation, the authors demonstrate that the *Adiponectin*-Cre transgene targets a subset of adipose stromal vascular cells in fetal inguinal WAT. These targeted stromal cells likely represent actively differentiating or highly committed preadipocytes. This stands in contrast to the expression pattern of Cre in adult *Adiponectin*-Cre mice. In postnatal WAT depots, Cre expression is restricted to fully mature adipocytes [37].

We independently confirmed and extended the results of Hong et al. by analyzing Cre-dependent reporter expression in *Adiponectin*-Cre; *Rosa26R*^{loxP-stop-loxP-tdTomato} mice (Supplementary Figure 2a). We isolated the stromal vascular fraction (SVF) from inguinal WAT of E18.5 embryos and analyzed the adipose progenitor pool (*Pdgfra*⁺; CD45⁻; CD31⁻) by flow cytometry (Supplementary Figure 2b). Consistent with the results described by Hong et al., a subset of the *Pdgfra*⁺ population was tdTomato⁺ (Supplementary Figure 2d). Moreover, a vast majority of tdTomato⁺ cells actively expressed *Pdgfra* (Supplementary Figure 2e). Not all *Pdgfra*⁺ cells were targeted by *Adiponectin*-Cre at this particular stage; however, Hong et al. have demonstrated that these *Adiponectin*-Cre targeted cells proliferate and are highly adipogenic [38]. Of note, *Adiponectin*-Cre targeted precursors were only found in fetal inguinal WAT; tdTomato⁺ precursors were not found in SVF of adult WAT (Supplementary Figures 2f and g) or in the SVF of developing gonadal WAT at postnatal day 6 (P6) (Supplementary Figure 2h). These data indicate that during fetal inguinal WAT development, the *adiponectin* promoter is active at an earlier stage of the differentiation program than previously recognized. In contrast, *adiponectin* expression after birth is restricted to mature lipid-laden adipocytes.

Based on this observation and aforementioned published results, we reasoned that the *adiponectin*-Cre transgene would target floxed alleles in either the fetal precursor stage or as cells are actively undergoing differentiation. This would allow for targeted disruption of *Zfp423* in the developing inguinal WAT depot and provide a tool to investigate the function of *Zfp423* during the terminal differentiation of adipocytes and fetal development of inguinal WAT. Thus, we bred *adiponectin*-Cre transgenic mice with *Zfp423*^{loxP/loxP} animals (*Adiponectin*-Cre; *Zfp423*^{loxP/loxP} animals, denoted herein as *Zfp423*-AKO mice) (Figure 1A). *Zfp423*-AKO mice were born in the expected

Mendelian ratio and exhibited similar growth rate in comparison to control littermates. However, mRNA levels of *Pparγ2* and other adipocyte-selective genes in both inguinal WAT and fractionated inguinal adipocytes were significantly lower in *Zfp423*-AKO mice (Figure 1B; Supplementary Figure 3a). Histological analysis of inguinal fat depots isolated from *Zfp423*-AKO animals revealed the appearance of patches of adipocytes, which were smaller in size, loaded with less lipid, and lacked the signature unilocular white adipocyte morphology (Figure 1C–J). This phenotype differs significantly from the inducible model in which adipocyte-specific deletion of *Zfp423* induced in adult mice leads to a robust white-to-beige adipocyte conversion (~200-fold increase in *Ucp1* mRNA), without impacting the fat cell phenotype *per se* [31]. In sharp contrast, the expression of thermogenic genes *Ucp1*, *Cidea*, and *Prdm16* in iWAT of *Zfp423*-AKO mice was only marginally higher (<2-fold) than the expression found in controls (Supplementary Figures 3a and b). The lower expression of *Pparγ* and other adipocyte-selective genes in purified adipocytes suggests that fetal inguinal adipocytes fail to fully undergo terminal differentiation in the absence of *Zfp423*. These data suggest that indeed Cre activity occurs at an earlier stage of the adipocyte life cycle than it does in adult mice and that the formation of a fully mature adipocyte is needed before *Zfp423*-deficiency can trigger an induction of the thermogenic gene program.

Next, we assessed the overall functionality of the inguinal WAT depot in control and *Zfp423*-AKO mice. First, we tested the responsiveness of adipose depots to insulin stimulation, as reflected by the activation of its downstream signal transducer, Akt (phosphorylated-AKT). As compared to control animals, insulin-induced Akt phosphorylation was significantly impaired in the inguinal WAT of *Zfp423*-AKO mice (Figure 1K). Moreover, the lipolytic capacity of *Zfp423*-deficient adipose tissue was impaired. Isolated inguinal WAT depots from *Zfp423*-AKO mice released significantly less glycerol as compared to control inguinal WAT upon stimulation by the β₃-adrenergic receptor agonist CL316243 (Figure 1L). These data provide functional evidence that inguinal WAT depots of *Zfp423*-AKO mice are not fully mature and developed.

Levels of *Zfp423* were significantly lower in the gonadal WAT depot as well as the interscapular brown adipose tissue depot of *Zfp423*-AKO mice (Supplementary Figures 3c and d), consistent with the known activity of the *adiponectin*-Cre transgene in all adipose depots. However, none of the abnormalities observed in the inguinal WAT depots of *Zfp423*-AKO mice was found in the gonadal WAT depot or interscapular brown adipose tissue (BAT) depot (Supplementary Figures 3c–h). This could imply a depot-selective requirement of *Zfp423* during adipose tissue development. However, based on the differential activity of the *adiponectin*-Cre transgene in precursors of different depots, Cre-mediated deletion of *Zfp423* likely occurred later in the differentiation program of gonadal white adipocytes and interscapular brown adipocytes. In fact, the expression of the thermogenic gene program was elevated in the gWAT of *Zfp423*-AKO mice (Supplementary Figure 3c), similar to the gonadal WAT phenotype found in the previously reported inducible adult adipocyte-specific *Zfp423* knockout model. Baseline levels of these same thermogenic genes in the BAT were not impacted by the loss of *Zfp423* (Supplementary Figure 3d).

3.3. Developmental defects caused by *Zfp423*-deficiency are cell autonomous and can be rescued by *Pparγ* agonism

Next, we evaluated whether the observed defects in inguinal WAT development and function were largely due to a cell autonomous role for *Zfp423* in adipocyte differentiation. We isolated and established

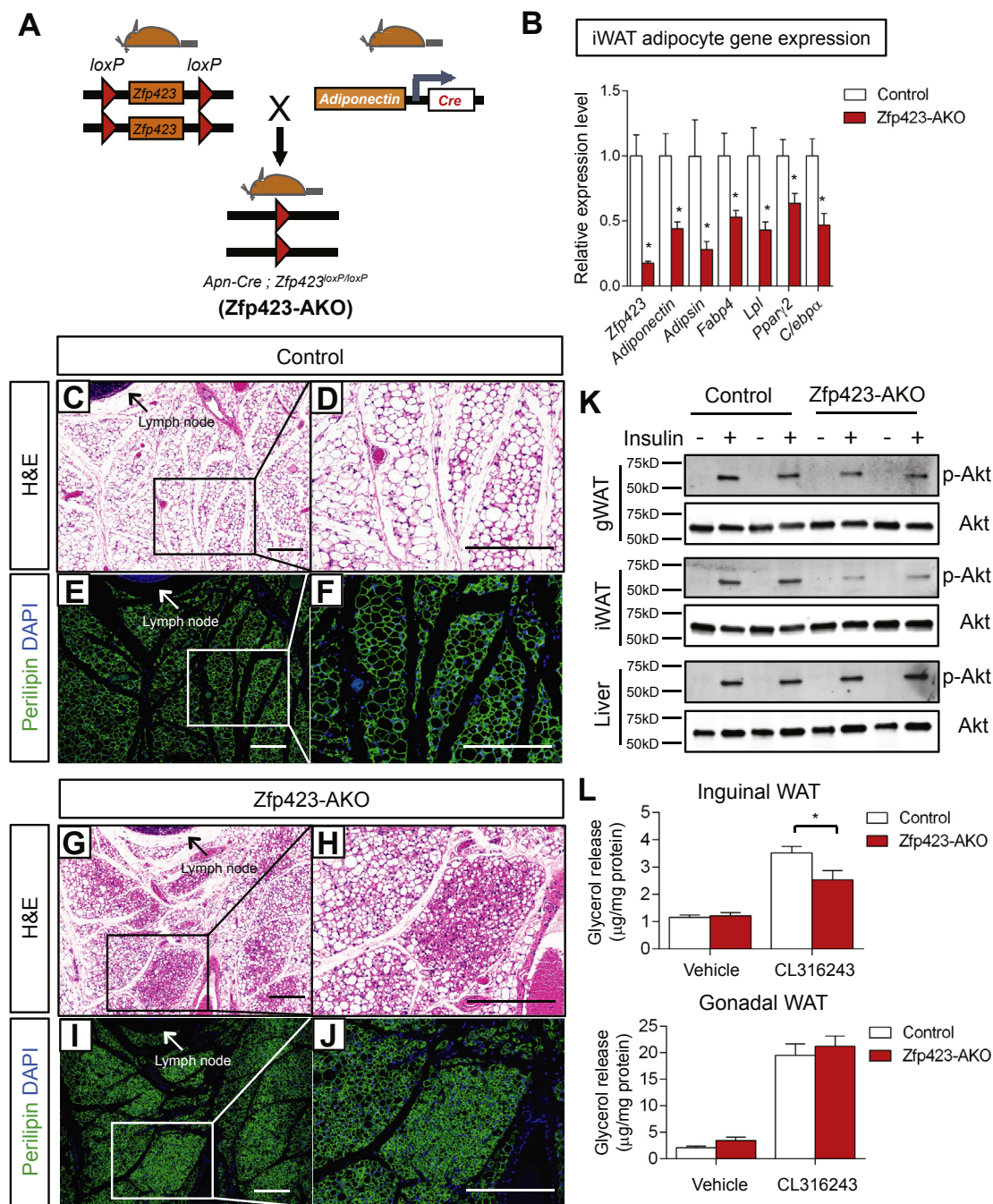


Figure 1: Inguinal adipose tissue development is impaired in *Adiponectin-Cre; Zfp423^{loxP/loxP}* mice. (A) *Adiponectin-Cre; Zfp423^{loxP/loxP}* (*Zfp423*-AKO) mice are generated by breeding *Adiponectin-Cre* transgenic mice to animals carrying floxed *Zfp423* alleles (*Zfp423^{loxP/loxP}*). (B) Relative mRNA levels of *Zfp423* and indicated adipocyte genes in fractionated inguinal white adipose tissue (iWAT) adipocytes from 8 weeks-old control and *Zfp423*-AKO mice. * denotes $p < 0.05$ from student's t-test. $n = 5$ mice. (C–F) Representative H&E staining (c, d) and perilipin immunofluorescence staining (e, f) of iWAT sections obtained from 8 weeks-old control mice. Scale bar, 200 μ m. (G–J) Representative (g, h) H&E staining and (i, j) perilipin immunofluorescence staining of iWAT sections obtained from 8 weeks-old *Zfp423*-AKO mice. Scale bar, 200 μ m. (K) Western blot analysis of phosphorylated-Akt (p-Akt) and total Akt protein levels in tissue extracts of gonadal WAT (gWAT), iWAT, and liver of 8 weeks-old control and *Zfp423*-AKO mice administered with insulin (1 U/kg). (L) β 3-adrenergic receptor induced lipolysis (measured as glycerol release) in *ex vivo* diced iWAT and gWAT isolated from 8 weeks-old control and *Zfp423*-AKO mice. * $p < 0.05$ from two-way ANOVA. $n = 6$ mice.

cultures of the stromal vascular fraction (SVF) of inguinal WAT of control and *Zfp423*-AKO mice. *In vitro* adipocyte differentiation from cultured cells was induced using the standard 3T3-L1 adipogenic cocktail containing dexamethasone, IBMX and insulin. Differentiated cultures from both genotypes appeared equally capable of

accumulating lipid, as indicated by Oil Red O staining (Figure 2A). However, mRNA levels of *Ppar γ 2* and other genes selective to mature adipocytes (*adiponectin*, *adipsin*, and *C/ebpa*) were consistently reduced in the *Zfp423*-deficient cells (Figure 2B). These data suggest that the loss of *Zfp423* expression after the onset of adiponectin/Cre

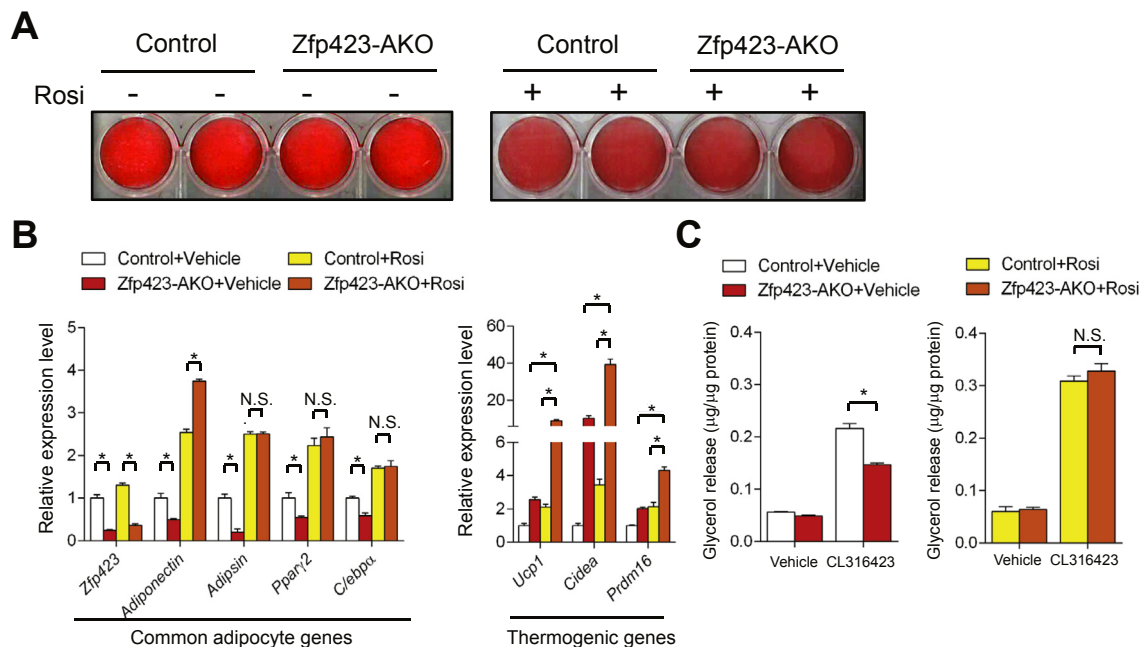


Figure 2: Developmental defects caused by *Zfp423*-deficiency are cell autonomous and can be rescued by *Pparγ* agonism. (A) Oil Red O staining of *in vitro* derived adipocytes differentiated from cultures of the inguinal stromal vascular fraction of control and *Zfp423*-AKO mice. Cultures were treated with vehicle (–) or rosiglitazone (+) throughout differentiation. **(B)** Relative mRNA levels of common adipocyte genes and thermogenic genes in adipocytes cultures differentiated as shown in (a). * denotes $p < 0.05$ from two-way ANOVA. N.S. denotes not statistically significant. $n = 4$ for all conditions. **(C)** β_3 -adrenergic receptor induced lipolysis in *in vitro* derived control and *Zfp423*-AKO white adipocytes treated with vehicle or rosiglitazone during differentiation. * denotes $p < 0.05$ from two-way ANOVA. N.S. denotes not statistically significant. $n = 3$ mice.

expression leads to arrested terminal differentiation. Consistent with the observations made *in vivo*, β_3 -adrenergic agonist-induced glycerol release was attenuated in *Zfp423*-deficient cells, suggesting *Zfp423*-deficient cells were functionally defective in terms of lipolytic ability (Figure 2C). Collectively, these results provide evidence that *Zfp423* is required for the terminal differentiation of inguinal white adipocytes and the fetal development of this WAT depot.

We previously reported that *Zfp423* regulates *Pparγ* expression in 3T3 fibroblast cell lines [30]. Consistent with these data, *Pparγ2* expression was lower in freshly isolated or *in vitro* derived *Zfp423*-deficient adipocytes from *Zfp423*-iAKO mice (Figures 1B and 2B). However, *Pparγ* expression in *Zfp423*-deficient adipocytes was not completely absent. Thus, we asked whether agonism of the remaining *Pparγ* in *Zfp423* knockout adipocytes is sufficient to rescue the defects in white adipocyte differentiation and function. First, we performed *in vitro* differentiation assays with the *Pparγ* agonist rosiglitazone added to the differentiation media. Under this condition, adipocyte cultures from both groups appeared equally differentiated (Figure 2A); no statistically significant differences in mRNA levels of adipocyte-selective genes were observed (Figure 2B). Moreover, the CL316423-induced lipolytic capacity of *Zfp423*-deficient cells was restored by rosiglitazone treatment (Figure 2C), suggesting that the rescue of *Pparγ* activity by its agonist was largely sufficient to correct the differentiation defects caused by *Zfp423*-deficiency. Consistent with this observation, the expression of the thermogenic gene program in rescued *Zfp423*-deficient adipocyte cultures is strongly induced (Figure 2B). This phenotype is now similar to adipocyte cultures in which *Zfp423* is inactivated post-differentiation.

We also tested the ability of rosiglitazone to rescue the observed defects in inguinal WAT development *in vivo*. Inguinal adipocytes begin to appear around embryonic day 16 (E16) and most adipocytes are

formed by postnatal day 5 (P5) [35]. Thus, we administered vehicle or rosiglitazone to control and *Zfp423*-AKO animals from E16 to P5 via gavage of pregnant and lactating mothers (Figure 3A). At P5, iWAT from vehicle-treated *Zfp423*-AKO pups appeared poorly differentiated; numerous patches of small, lipid-devoid cells were apparent (Figure 3B–E), and levels of all adipocyte-selective genes were lower than in vehicle-treated control mice (Figure 3J). However, none of these developmental defects was observed in *Zfp423*-AKO pups exposed to rosiglitazone during the peri-natal period. Compared to iWAT from rosiglitazone-treated control mice, iWAT from rosiglitazone-treated knockout mice exhibits a normal morphology (Figure 3F–I) and expresses comparable levels of adipocyte-selective genes (Figure 3J). Thus, we reasoned that these rescued animals are now essentially similar to the aforementioned model in which *Zfp423* is inactivated in adipocytes of adult mice. Indeed, the thermogenic gene program was strongly induced in the rescued *Zfp423*-AKO mice (Figure 3K). Altogether, these data provide genetic evidence that *Zfp423* is a critical regulator of the fetal development of inguinal white adipose tissue, serving as an upstream activator of *Pparγ* expression.

3.4. Inguinal WAT of *Zfp423*-deficient mice undergoes a pathological adipose tissue expansion upon high-fat diet feeding

In the setting of caloric excess, a lack of functional adipocytes can lead to inappropriate lipid handling in adipose tissue and/or altered adipokine production. This can subsequently lead to an accumulation of lipids in non-adipose organs. Ectopic storage of lipids can be deleterious (“lipotoxicity”) and trigger the development of insulin resistance [39]. The poor development of the inguinal WAT depot in *Zfp423*-AKO mice prompted us to challenge the animals with an obesogenic high-fat diet (60% kcal from fat). Control and littermate male *Zfp423*-AKO mice were administered high-fat diet feed beginning from 5 weeks of

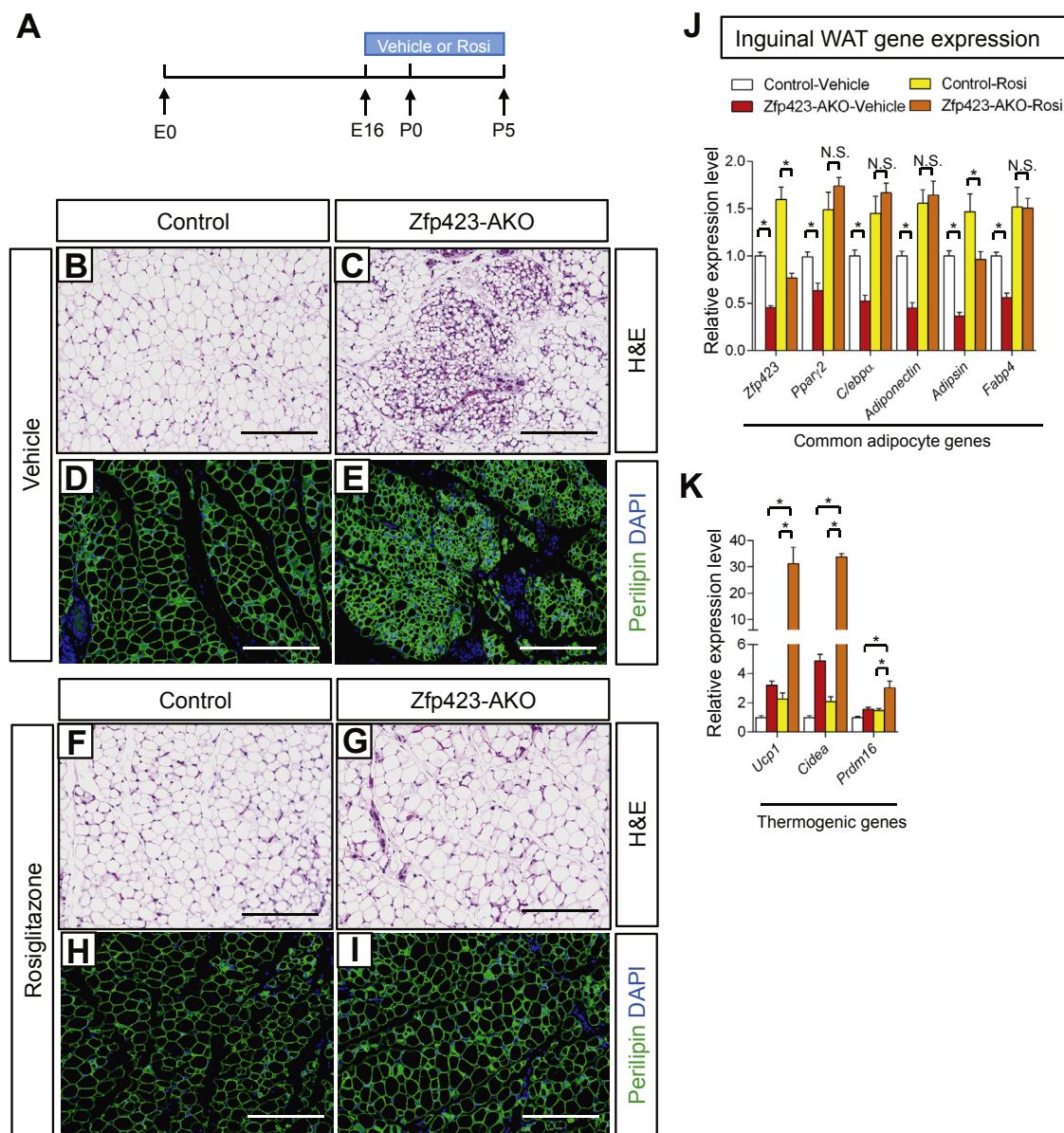


Figure 3: Fetal Inguinal WAT development in *Adiponectin-Cre; Zfp423^{loxP/loxP}* mice is corrected by perinatal administration of the Ppar γ agonist, Rosiglitazone. (A) Vehicle or the Ppar γ agonist, rosiglitazone (Rosi), was delivered to pregnant/lactating mothers (10 mg kg⁻¹/day) from embryonic day (E) 16 (E16) to postnatal (P) day 5 (P5). Offspring were harvested for analysis at P5. (B, E) Representative H&E staining (B, C) and perilipin immunofluorescence staining (D, E) of iWAT sections obtained from 5 days-old control and Zfp423-AKO pups treated with vehicle. Scale bar, 200 μ m. (F, I) Representative H&E staining (F, G) and perilipin immunofluorescence staining (H, I) of iWAT sections obtained from 5 days-old control and Zfp423-AKO pups treated with rosiglitazone. Scale bar, 200 μ m. (J) Relative mRNA levels of common adipocyte genes in iWAT from 5 days-old control and Zfp423-AKO pups treated with vehicle or rosiglitazone. * denotes $p < 0.05$ from two-way ANOVA. N.S. denotes not statistically significant. $n = 6$ mice. (K) Relative mRNA levels of thermogenic genes in iWAT from 5 days-old control and Zfp423-AKO pups treated with vehicle or rosiglitazone. * denotes $p < 0.05$ from two-way ANOVA. $n = 6$ mice.

age. The control and *Zfp423*-deficient mice equally gained weight over the first 8 weeks of the high-fat diet regimen (Figure 4A). Afterwards, *Zfp423*-deficient animals gained slightly more weight than controls; however, by the end of the 16 week period, these differences in weight measurements did not reach statistical significance (Figure 4A). Analysis of *Zfp423* knockout mice at 8 weeks of age revealed differences in adipose tissue size and morphology. Weights of inguinal, but not gonadal or mesenteric, fat depots of *Zfp423*-deficient mice were higher than the weights of control inguinal adipose tissues (Figure 4B). Histological analysis revealed a striking inguinal WAT phenotype with

hallmarks of unhealthy adipose expansion (Figure 4C and D). Many small adipocytes devoid of lipids were observed in knockout animals, similar to what was observed in depots from chow-fed animals. However, the frequency of large, hypertrophic adipocytes was greater in the *Zfp423*-AKO mice (Figure 4E). Overall, the average adipocyte size was approximately 40% higher than found in controls (Figure 4F). This hypertrophic adipose phenotype was accompanied by increased inflammation, as assessed by the increased presence of crown-like immune structures (Figure 4G). Moreover, higher expression levels of immune cell selective genes and relatively lower expression of

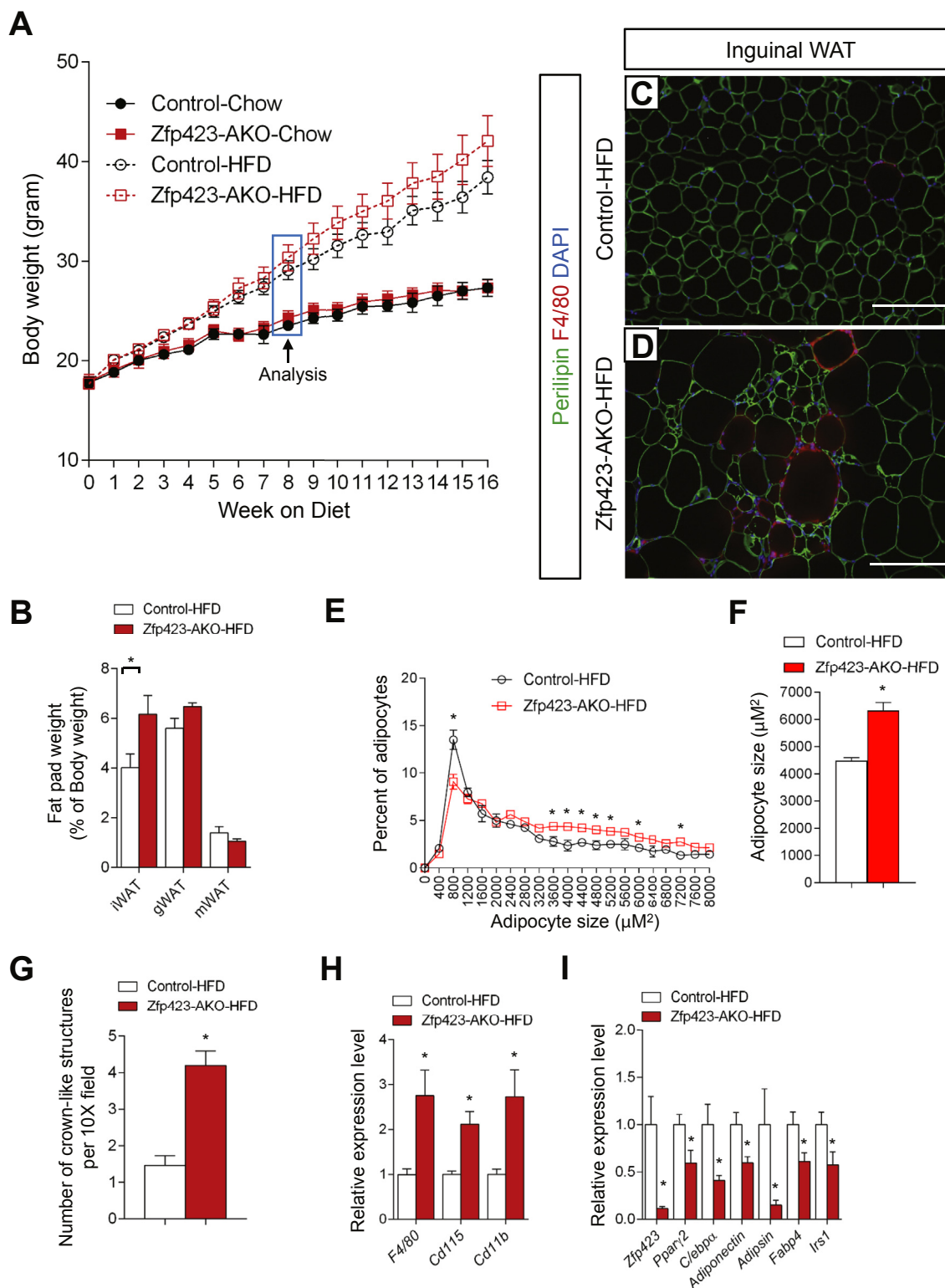


Figure 4: High-fat diet feeding leads to a pathological inguinal WAT expansion in *Adiponectin-Cre*, *Zfp423^{loxP/loxP}* mice. (A) Weekly body weight measurements of control and Zfp423-AKO mice fed chow or high-fat diet (HFD) for 16 weeks following weaning. $n = 6-8$ mice. (B) Adipose depot mass (normalized to body weight) of control and Zfp423-AKO mice after 8 weeks of HFD feeding. $*p < 0.05$ from student's test. $n = 6-8$ mice. (C, D) Representative immunofluorescence images of Perilipin (green) and F4/80 (red) expression in iWAT paraffin sections obtained from control and Zfp423-AKO mice after 8 weeks of HFD feeding. Scale bar, 200 μm . (E) Distribution of adipocyte size in control and Zfp423-AKO iWAT after 8 weeks of HFD feeding. $*$ denotes $p < 0.05$ from two-way ANOVA. $n = 6-8$ mice. (F) Average adipocyte size of control and Zfp423-AKO iWAT after 8 weeks of HFD feeding. $*$ denotes $p < 0.05$ from student's test. $n = 6-8$ mice. (G) Number of crown-like structures (F4/80 positive) in control and Zfp423-AKO iWAT after 8 weeks of HFD feeding. $*$ denotes $p < 0.05$ from student's test. $n = 6-8$ mice. (H-I) Relative mRNA levels of macrophage markers (H) and adipocyte-selective genes (I) in control and Zfp423-AKO iWAT after 8 weeks of HFD feeding. $*$ denotes $p < 0.05$ from student's test. $n = 6$ mice.

adipocyte-selective genes were detected in total inguinal WAT tissue (Figure 4H and I). After 8 weeks of high-fat diet feeding, the gonadal WAT appeared similar in mass to corresponding depots from control animals (Figure 4B). No significant differences in gonadal adipocyte cell size were observed between the two groups (Supplementary Figure 4a). However, there was an abundance of crown-like structures in this depot of *Zfp423*-AKO mice (Supplementary Figures 4b and c), correlating with increased expression of immune cell transcripts in whole gonadal white adipose tissue (Supplementary Figure 4d). Chronic adipose inflammation is typically associated with adipose tissue dysfunction. Indeed, in *Zfp423*-AKO mice, insulin-stimulated AKT phosphorylation was blunted in both inguinal and gonadal WAT depots (Supplementary Figure 4f), and serum levels of adiponectin were significantly lower after 8 and 16 weeks of high-fat diet feeding (Supplementary Figure 4g).

Unhealthy adipose tissue expansion is often associated with systemic alterations in nutrient handling. Consistent with this notion, we observed higher levels of serum triglycerides in *Zfp423*-AKO mice than in controls, both after 8 and 16 weeks of high-fat diet feeding (Figure 5A and B). This correlated with a progressive increase in hepatic steatosis (Figure 5C–F) and resistance to insulin-induced AKT activation (Figure 5G) in the knockout animals. Glucose and insulin tolerance tests revealed systemic impairments in glucose homeostasis in *Zfp423*-AKO mice. *Zfp423*-AKO mice were less glucose tolerant than control animals and less sensitive to the actions of insulin (Figure 5H and I). All together, the ectopic lipid accumulation, lower serum adiponectin levels, glucose intolerance, and insulin resistance indicate that obese *Zfp423*-deficient animals exhibit the metabolic profile commonly observed in lipodystrophy.

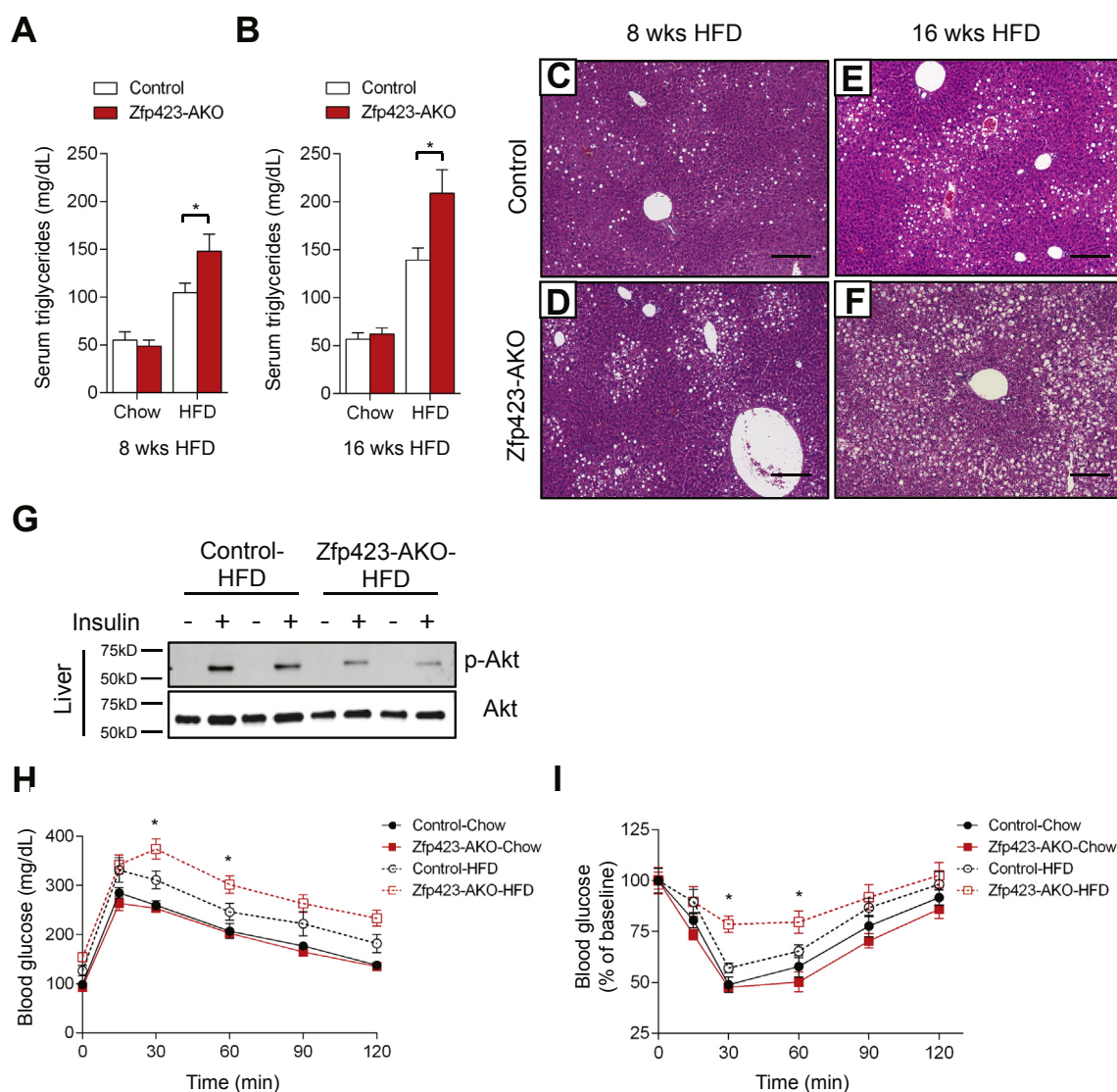


Figure 5: Obese *Adiponectin-Cre*, *Zfp423*^{loxP/loxP} mice are insulin resistant and have increased hepatic steatosis. (A, B) Serum triglyceride levels in control and *Zfp423*-AKO mice after 8 (A) or 16 weeks (B) of chow or HFD feeding. * denotes $p < 0.05$ from two-way ANOVA. $n = 6-8$ mice. (C, D) Representative H&E staining of livers from control (C) and *Zfp423*-AKO (D) mice after 8 weeks of HFD feeding. Scale bar, 200 μm . (E, F) Representative H&E staining of livers from control (E) and *Zfp423*-AKO (F) mice after 16 weeks of HFD feeding. Scale bar, 200 μm . (G) Western blot analysis of phosphorylated-Akt (p-Akt) and total Akt protein levels in liver extracts from 8 week HFD-fed control and *Zfp423*-AKO mice administrated with insulin (2 U/kg). (H) Glucose tolerance test of control and *Zfp423*-AKO mice after 8 weeks HFD feeding. * denotes $p < 0.05$ from Two-way ANOVA. $n = 6-8$ mice. (I) Insulin tolerance test of control and *Zfp423*-AKO mice after 8 weeks HFD feeding. * denotes $p < 0.05$ from Two-way ANOVA. $n = 6-8$ mice.

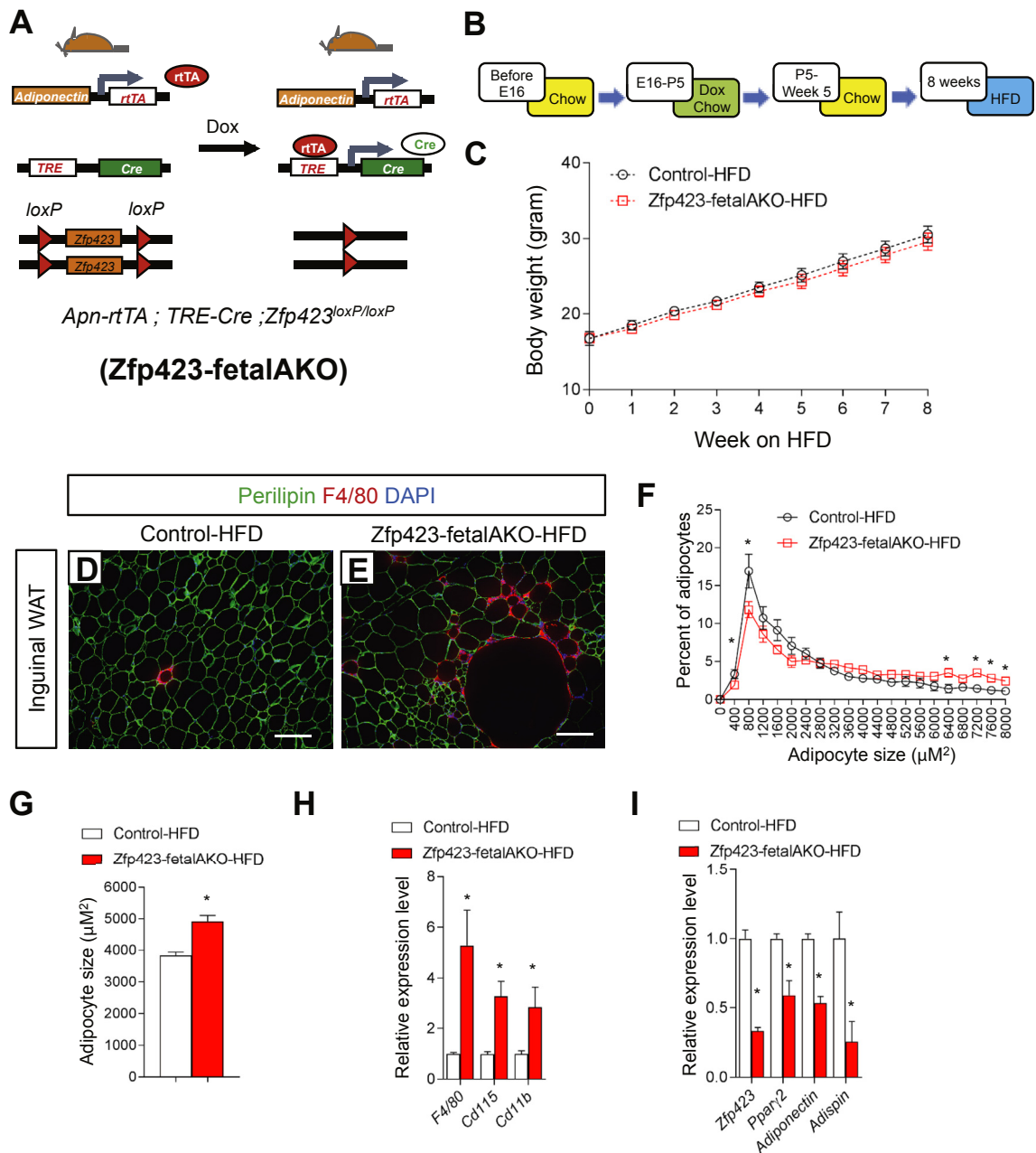


Figure 6: Transient fetal exposure of *Adiponectin*-rTA; *TRE*-Cre; $Zfp423^{loxP/loxP}$ animals leads to inguinal white adipose depot-selective targeting of *Zfp423*. (A) Inducible inactivation of *Zfp423* in *adiponectin*-expressing cells is achieved by breeding the *adiponectin*-rTA transgenic mice to animals expressing Cre recombinase under the control of the Tet-response element (*TRE*-Cre) and carrying floxed *Zfp423* alleles ($Zfp423^{loxP/loxP}$). Littermates carrying only *adiponectin*-rTA and $Zfp423^{loxP/loxP}$ alleles (i.e. Cre⁻) were used as the control animals. Exposure of animals to doxycycline from E16 to P5 via feeding of mothers results in a model of selective *Zfp423* inactivation in the developing inguinal WAT (Zfp423-fetalAKO mice). (B) Control and Zfp423-fetalAKO mice were exposed to doxycycline from E16 to P5 and then kept on standard chow diet until 5 week old before switching to HFD for another 8 weeks. (C) Weekly body weight measurements of control and Zfp423-fetal AKO mice during 8 weeks of HFD feeding. $n = 6$ mice. (D, E) Representative immunofluorescence images of perilipin (green) and F4/80 (red) expression in iWAT paraffin sections from control (D) and Zfp423-fetalAKO (E) mice after 8 weeks of HFD feeding. Scale bar, 200 μm . (F) Distribution of adipocyte size in control and Zfp423-fetalAKO iWAT after 8 weeks of HFD feeding. * denotes $p < 0.05$ from two-way ANOVA. $n = 6$ mice. (G) Average adipocyte size in control and Zfp423-fetalAKO iWAT after 8 weeks of HFD feeding. * denotes $p < 0.05$ from student's t-test. $n = 6$ mice. (H, I) Relative mRNA levels of macrophage markers (H) and adipocyte-selective genes (I) in control and Zfp423-fetalAKO iWAT after 8 weeks of HFD feeding. * denotes $p < 0.05$ from student's t-test. $n = 6$ mice.

3.5. Pathological expansion of subcutaneous WAT is sufficient to trigger gonadal WAT dysfunction and impaired systemic nutrient homeostasis

Defects in adipose development in Zfp423-AKO mice were restricted to the subcutaneous inguinal WAT depot; however, upon high-fat diet

feeding, systemic insulin resistance was apparent and gonadal WAT also appears dysfunctional. These data suggest that a pathological remodeling specifically of subcutaneous WAT in obesity is sufficient to drive intra-abdominal WAT dysfunction and systemic nutrient imbalance. In order to test this hypothesis, we utilized our doxycycline-

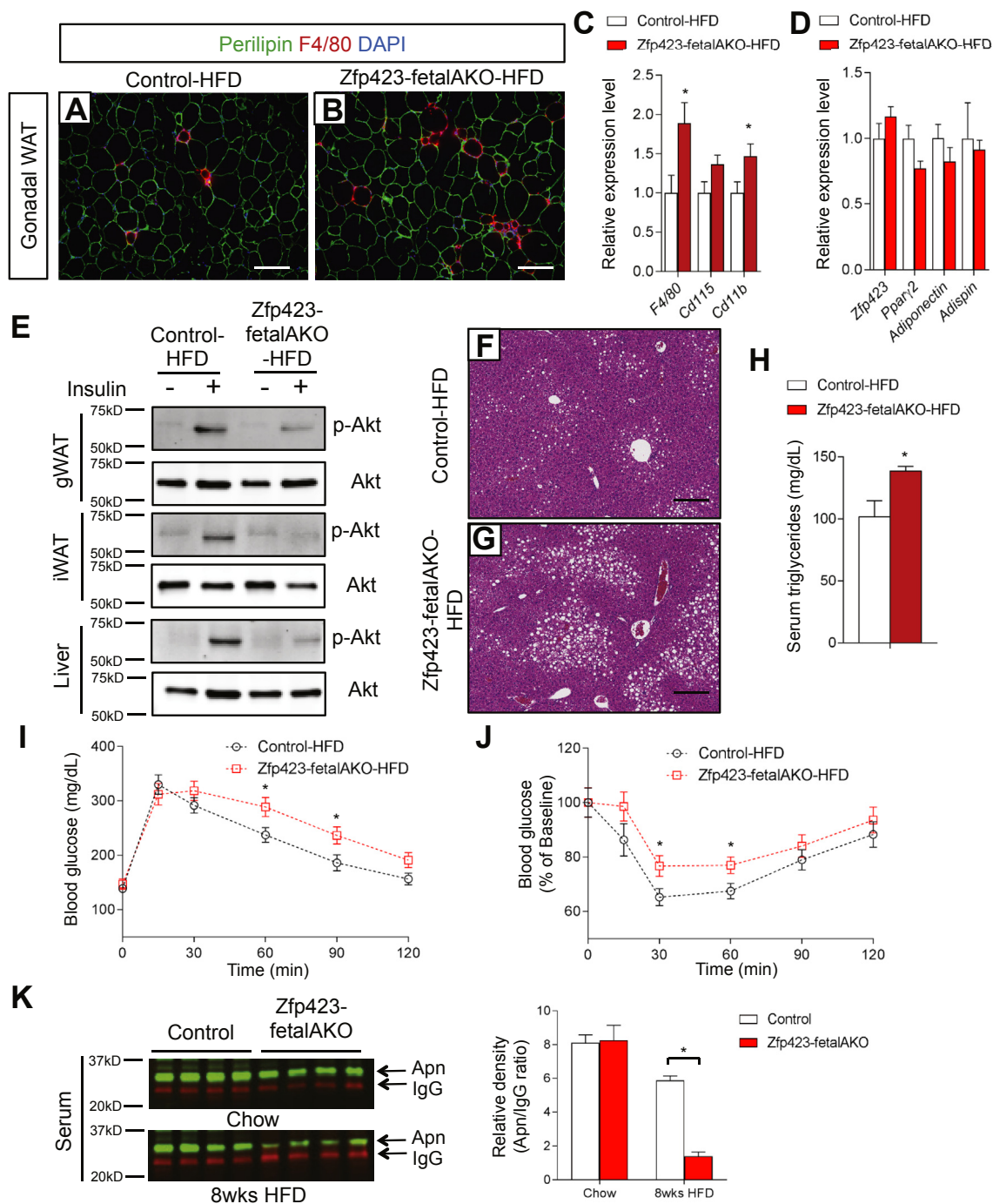


Figure 7: Pathological expansion of subcutaneous WAT is sufficient to trigger impaired systemic nutrient homeostasis. (A, B) Representative immunofluorescence images of perilipin (green) and F4/80 (red) expression in sections of gWAT from control and Zfp423-fetalAKO mice after 8 weeks of HFD feeding. Scale bar, 200 μ m. **(C, D)** Relative mRNA levels of macrophage markers **(C)** and adipocyte-selective genes **(D)** in gWAT of control and Zfp423-fetalAKO mice after 8 weeks of HFD feeding. * denotes $p < 0.05$ from student's t-test. $n = 6$ mice. **(E)** Western blot analysis of phosphorylated-Akt (p-Akt) and total Akt protein levels in tissue extracts of gWAT, iWAT, and liver of HFD-fed control and Zfp423-fetalAKO mice administrated with insulin (2 U/kg). **(F, G)** Representative H&E staining of livers from control and Zfp423-fetalAKO mice after 8 weeks of HFD feeding. Scale bar, 200 μ m. **(H)** Serum triglyceride levels in control and Zfp423-fetalAKO mice after 8 weeks of HFD feeding. * denotes $p < 0.05$ from student's t-test. $n = 6$ mice. **(I)** Glucose tolerance test of control and Zfp423-fetalAKO mice after 8 weeks HFD feeding. * denotes $p < 0.05$ from student's t-test. $n = 6$ mice. **(J)** Insulin tolerance test of control and Zfp423-fetalAKO mice after 8 weeks HFD feeding. * denotes $p < 0.05$ from student's t-test. $n = 6$ mice. **(K)** Western blot analysis and quantification of serum adiponectin levels in control and Zfp423-fetalAKO mice fed with chow or HFD for 8 weeks starting at 5 weeks of age. For quantification, intensity of adiponectin band is normalized to that of IgG band. * denotes $p < 0.05$ from two-way ANOVA. $n = 4$ mice.

inducible, adipose-specific, *Zfp423* knockout model (Zfp423-iAKO mice) (Figure 6A). Wang et al. previously demonstrated that fetal exposure of doxycycline to *Adiponectin*-rtTA; TRE-Cre; *Rosa26^{lacZ}* pups specifically during E16 through P5 of life results in adipose depot-selective gene targeting [35]. The inguinal WAT depot, and to a lesser extent the classic BAT depots, express the *Adiponectin*-rtTA transgene during this period. However, gonadal and other intra-abdominal WAT depots are not yet formed at this stage and thus are not targeted. Thus, we administered doxycycline-containing chow diet to pregnant/lactating mice carrying control (*Adiponectin*-rtTA; *Zfp423^{loxP/loxP}*) and *Zfp423*-iAKO mice (*Adiponectin*-rtTA; TRE-Cre; *Zfp423^{loxP/loxP}*) specifically during E16 to P5 of life and then harvested animals at 5 weeks of age for analysis (Figure 6A). As expected, *Zfp423* mRNA levels were significantly reduced in the inguinal WAT depot and interscapular BAT of *Zfp423*-iAKO mice (Supplementary Figure 5a). However, levels of *Zfp423* in the gonadal WAT were not reduced (Supplementary Figure 5b). Similar to the *Zfp423*-AKO mice described above, the inguinal WAT did not appear fully developed, as revealed by the large regions of undifferentiated cells (Supplementary Figures 5d and e) and the lower expression of adipocyte-selective genes in the tissue (Supplementary Figure 5a). Importantly, brown adipose tissue and gonadal WAT appeared indistinguishable from controls (Supplementary Figure 5c, f–i).

At five weeks of age we challenged the inducible *Zfp423* knockout model (herein, “*Zfp423*-fetalAKO”) to high-fat diet feeding (Figure 6B). After 8 weeks of high-fat diet feeding, many of the phenotypes

observed in the obese *Zfp423*-AKO mice were again apparent. Body weights of *Zfp423*-fetalAKO mice were indistinguishable from control animals (Figure 6C); however, inguinal WAT had an unhealthy appearance, characterized by adipocyte hypertrophy, increased inflammation, and lower levels of adipocyte-selective transcripts (Figure 6D–I). The expression levels of *Zfp423* and other adipocyte genes remained unaltered in *Zfp423*-fetalAKO gWAT (Figure 7D); however, there was an abundant number of crown-like structures, correlating with the elevated levels of transcripts encoding immune cell markers in the gonadal depot of the knockout mice (Figure 7A–C). Functionally, both inguinal and gonadal WAT of the *Zfp423*-fetalAKO mice appeared relatively more resistant to the actions of insulin. Insulin-stimulated p-AKT induction was strongly blunted in both depots (Figure 7E). Hepatic insulin resistance was also apparent (Figure 7E), correlating with increased hepatic steatosis and serum triglycerides (Figure 7F–H). Intraperitoneal glucose and insulin tolerance tests revealed that *Zfp423*-fetalAKO mice were more glucose intolerant and insulin resistant than controls (Figure 7I and J). These phenotypes of *Zfp423*-fetalAKO mice may be explained, at least in part, by the largely reduced levels of serum adiponectin (Figure 7K). This model of inguinal-selective *Zfp423*-inactivation largely recapitulated the metabolic phenotype observed in *Zfp423*-AKO animals. These data strongly suggest that pathological subcutaneous WAT expansion in adult obesity, triggered initially by poor fetal adipocyte differentiation, is sufficient to considerably impair visceral WAT function and systemic glucose and lipid metabolism.

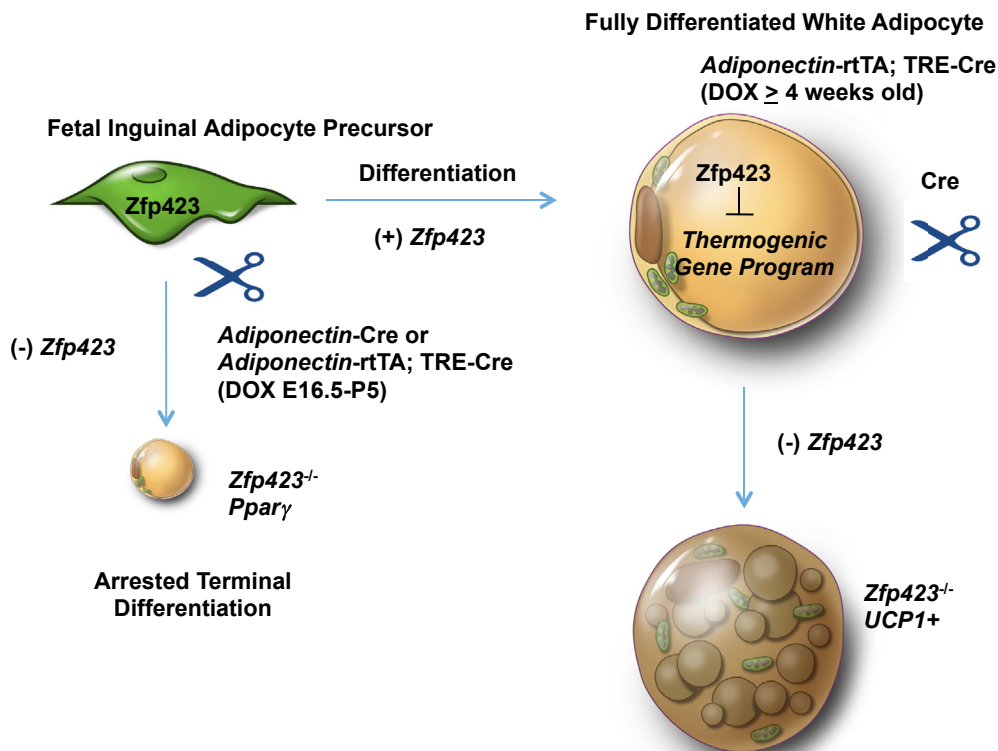


Figure 8: Establishment and Maintenance of the White Adipocyte Lineage by *Zfp423*. *Zfp423* expression identifies committed preadipocytes and drives adipocyte differentiation through activation of *Ppar γ* [28–30]. Cre-mediated inactivation of *Zfp423* in developing fetal inguinal WAT precursors results in arrested terminal adipocyte differentiation. In fully differentiated white adipocytes, *Zfp423* functions to suppress the thermogenic gene program, thereby maintaining the white adipocyte phenotype. Inducible, Cre-mediated inactivation of *Zfp423* in fully differentiated white adipocytes of adult mice leads to a lineage reprogramming in which mature white adipocytes are converted to thermogenic UCP1-expressing beige-like adipocytes [31].

4. DISCUSSION

We recently demonstrated that *Zfp423* maintains the mature white adipocyte phenotype through suppression of the adipocyte thermogenic gene program. This was demonstrated by targeting mature adipocytes in adult animals through use of the doxycycline-inducible *Adiponectin*-rtTA transgene. Here, we use the same genetic system or the commonly used constitutively active *Adiponectin*-Cre allele and observe a vastly different phenotype when gene ablation is induced during fetal adipose development. When *Zfp423* is removed from mature adipocytes of adult animals, a white-to-beige phenotypic switch is observed. When *Zfp423* is removed from precursors and/or actively differentiating cells, we observe a defect in the terminal differentiation of fetal white adipocytes (Figure 8). This is apparent by the lack of lipid accumulation and lower expression of *Ppar γ* and adipocyte-selective genes. The inability of the thermogenic gene program to activate in these *Zfp423*-deficient cells is likely due to the reduction in *Ppar γ* expression. This discrepancy in the phenotypes is likely attributable to the fact that *Adiponectin*-Cre is active during fetal inguinal adipocyte differentiation while only active in fully mature adipocytes in adult animals. These data highlight the emerging notion that fetal adipose precursors appear distinct from adult adipose precursors, highlighted in part by the expression of *adiponectin*, *perilipin*, and perhaps other genes [38,40]. Moreover, these data highlight a critical role for *Zfp423* in both the establishment and maintenance of the white adipose lineage.

The data presented here highlight some of the pros and cons of the various genetic tools now available for manipulating genes within the adipose lineage. The *Pdgfra*-Cre line targets the adipose precursors and descending adipocytes with high efficiency; however, use of these mice as a tool may depend on the expression pattern of the floxed gene of interest. The *Adiponectin*-Cre line developed by Rosen and colleagues is undoubtedly the most specific and efficient tool for adipose targeting [41]; however, the data here highlight that Cre-mediated recombination in these mice is not entirely confined to fully differentiated adipocytes. During fetal inguinal WAT development, Cre expression occurs in cells that are most likely either highly committed preadipocytes or actively differentiating cells. Further analysis of these cells will be needed to understand their properties. After birth, Cre expression appears limited to mature, lipid-laden adipocytes, at least in the depots examined. Thus, the timing of Cre expression in the different depots of these animals has to be considered when interpreting results. As such, our results can only confirm an important role for *Zfp423* in the onset of fetal subcutaneous WAT development. *Zfp423* expression marks perivascular adipose precursors in adult mice; however the requirement of this factor in adult adipocyte differentiation *in vivo*, particularly in intra-abdominal depots, still remains unknown and will require the use of additional models. Importantly, models allowing inducible expression of Cre recombinase, such as the Tet-on system employed here, allow for gene function to be dissected at various stages of life. Furthermore, timing the doxycycline treatment allows white adipose depots to be targeted in a selective manner.

Clinical studies over the past decade have revealed a striking correlation between adipose tissue cellularity and metabolic health in the setting of obesity. The phenotypes of the *Zfp423*-AKO mice presented here fit well with clinical observations and highlight the importance of adipogenesis to healthy WAT remodeling and nutrient homeostasis in obesity. Poor fetal development of the inguinal WAT depot in *Zfp423* knockout mice leads to an expanded subcutaneous depot in obese

adults that resemble WAT depots of obese humans with metabolic syndrome. This pathological expansion is characterized by adipocyte hypertrophy, inflammation, and loss of insulin sensitivity. The observed adipocyte hypertrophy may be due to the observed defects in lipolytic capacity of the *Zfp423*-deficient adipocytes. It is also possible that remaining adipocytes become hypertrophied as an attempt to compensate for the lack of differentiated adipocytes. Clinically, and as observed in our animal models, these adipose phenotypes correlate with low serum adiponectin, high serum triglycerides, and systemic insulin resistance.

Adipose tissue distribution is also a reliable predictor of metabolic health. Preferential expansion of subcutaneous depots is often observed in the “healthy” obese populations. Interestingly, overall inguinal WAT mass was increased in the *Zfp423*-AKO mice. This suggests that subcutaneous adipose tissue quality is equally, if not more, important than adipose tissue quantity. This may also appear true for visceral adipose tissue. Senol-Cosar et al. recently reported that transgenic expression of tenomodulin in adipose tissue results in a healthy visceral WAT expansion, characterized by increased pre-adipocyte proliferation and lower inflammation and fibrosis, despite expanded gonadal WAT mass [42]. Our inguinal WAT-selective model of *Zfp423* ablation sheds further insight into the importance of healthy subcutaneous WAT by illustrating the systemic metabolic consequences of pathological subcutaneous adipose tissue expansion in obesity. A better understanding of how poor adipogenesis leads to pathological adipose remodeling may lead to novel therapeutic strategies to improve adipose tissue health in obesity.

ACKNOWLEDGEMENTS

The authors are grateful to members of the UTSW Touchstone Diabetes Center for useful discussions, and Drs. P. Scherer, C. Kusminski, and W. Holland for critical reading of the manuscript. The authors thank the UTSW Animal Resource Center, Metabolic Phenotyping Core, Pathology Core, Live Cell Imaging Core, and Flow Cytometry Core for excellent guidance and assistance with experiments performed here. This study was supported by NIDDK R03 DK099428, R01 DK104789, the Searle Scholars Program, the American Heart Association 15BGA22460021 to R.K.G., the American Heart Association postdoctoral fellowship 16POST26420136 to M.S., and the NIH NIGMS training grant T32 GM008203 to C.H.

CONFLICT OF INTEREST

All authors confirm that there are no known conflicts of interest associated with this publication and there has been no significant financial support for this work that could have influenced its outcome.

APPENDIX A. SUPPLEMENTARY DATA

Supplementary data related to this article can be found at <http://dx.doi.org/10.1016/j.molmet.2016.11.009>.

REFERENCES

- [1] Stern, J.H., Rutkowski, J.M., Scherer, P.E., 2016. Adiponectin, leptin, and fatty acids in the maintenance of metabolic homeostasis through adipose tissue crosstalk. *Cell Metabolism* 23(5):770–784.
- [2] Harms, M., Seale, P., 2013. Brown and beige fat: development, function and therapeutic potential. *Nature Medicine* 19(10):1252–1263.
- [3] Kissig, M., Shapira, S.N., Seale, P., 2016. SnapShot: brown and beige adipose thermogenesis. *Cell* 166(1), pp. 258–258 e1.

- [4] Cannon, B., Nedergaard, J., 2004. Brown adipose tissue: function and physiological significance. *Physiological Review* 84(1):277–359.
- [5] Unger, R.H., Clark, G.O., Scherer, P.E., Orci, L., 2010. Lipid homeostasis, lipotoxicity and the metabolic syndrome. *Biochimica et Biophysica Acta* 1801(3):209–214.
- [6] Appleton, S.L., Seaborn, C.J., Visvanathan, R., Hill, C.L., Gill, T.K., Taylor, A.W., et al., 2013. Diabetes and cardiovascular disease outcomes in the metabolically healthy obese phenotype: a cohort study. *Diabetes Care* 36(8):2388–2394.
- [7] Voulgari, C., Tentolouris, N., Dilaveris, P., Tousoulis, D., Katsilambros, N., Stefanadis, C., 2011. Increased heart failure risk in normal-weight people with metabolic syndrome compared with metabolically healthy obese individuals. *Journal of American College of Cardiology* 58(13):1343–1350.
- [8] Denis, G.V., Obin, M.S., 2013. 'Metabolically healthy obesity': origins and implications. *Molecular Aspects of Medicine* 34(1):59–70.
- [9] Lee, M.J., Wu, Y., Fried, S.K., 2013. Adipose tissue heterogeneity: implication of depot differences in adipose tissue for obesity complications. *Molecular Aspects of Medicine* 34(1):1–11.
- [10] Sun, K., Kusminski, C.M., Scherer, P.E., 2011. Adipose tissue remodeling and obesity. *Journal of Clinical Investigation* 121(6):2094–2101.
- [11] Klötting, N., Bluher, M., 2014. Adipocyte dysfunction, inflammation and metabolic syndrome. *Reviews in Endocrine Metabolic Disorders* 15(4):277–287.
- [12] Gealekman, O., Guseva, N., Hartigan, C., Apotheker, S., Gorgoglione, M., Gurav, K., et al., 2011. Depot-specific differences and insufficient subcutaneous adipose tissue angiogenesis in human obesity. *Circulation* 123(2):186–194.
- [13] Hardy, O.T., Perugini, R.A., Nicoloso, S.M., Gallagher-Dorval, K., Puri, V., Straubhaar, J., et al., 2011. Body mass index-independent inflammation in omental adipose tissue associated with insulin resistance in morbid obesity. *Surgery for Obesity and Related Disorders* 7(1):60–67.
- [14] Gustafson, B., Hedjazifar, S., Gogg, S., Hammarstedt, A., Smith, U., 2015. Insulin resistance and impaired adipogenesis. *Trends in Endocrinology & Metabolism* 26(4):193–200.
- [15] Gustafson, B., Hammarstedt, A., Hedjazifar, S., Smith, U., 2013. Restricted adipogenesis in hypertrophic obesity: the role of WISP2, WNT, and BMP4. *Diabetes* 62(9):2997–3004.
- [16] Gustafson, B., Gogg, S., Hedjazifar, S., Jenndahl, L., Hammarstedt, A., Smith, U., 2009. Inflammation and impaired adipogenesis in hypertrophic obesity in man. *American Journal of Physiology, Endocrinology and Metabolism* 297(5):E999–E1003.
- [17] Klötting, N., Fasshauer, M., Dietrich, A., Kovacs, P., Schon, M.R., Kern, M., et al., 2010. Insulin-sensitive obesity. *American Journal of Physiology, Endocrinology and Metabolism* 299(3):E506–E515.
- [18] Sun, K., Park, J., Gupta, O.T., Holland, W.L., Auerbach, P., Zhang, N., et al., 2014. Endotrophin triggers adipose tissue fibrosis and metabolic dysfunction. *Nature Communications* 5:3485.
- [19] Hardy, O.T., Czech, M.P., Corvera, S., 2012. What causes the insulin resistance underlying obesity? *Current Opinion in Endocrinology, Diabetes and Obesity* 19(2):81–87.
- [20] Kissebah, A.H., Krakower, G.R., 1994. Regional adiposity and morbidity. *Physiological Reviews* 74(4):761–811.
- [21] Tran, T.T., Yamamoto, Y., Gesta, S., Kahn, C.R., 2008. Beneficial effects of subcutaneous fat transplantation on metabolism. *Cell Metabolism* 7(5):410–420.
- [22] Kim, J.Y., van de Wall, E., Laplante, M., Azzara, A., Trujillo, M.E., Hofmann, S.M., et al., 2007. Obesity-associated improvements in metabolic profile through expansion of adipose tissue. *Journal of Clinical Investigation* 117(9):2621–2637.
- [23] Kusminski, C.M., Holland, W.L., Sun, K., Park, J., Spurgin, S.B., Lin, Y., et al., 2012. MitoNEET-driven alterations in adipocyte mitochondrial activity reveal a crucial adaptive process that preserves insulin sensitivity in obesity. *Nature Medicine* 18(10):1539–1549.
- [24] Cristancho, A.G., Lazar, M.A., 2011. Forming functional fat: a growing understanding of adipocyte differentiation. *Nature Reviews Molecular Cell Biology* 12(11):722–734.
- [25] Farmer, S.R., 2006. Transcriptional control of adipocyte formation. *Cell Metabolism* 4(4):263–273.
- [26] Rosen, E.D., Spiegelman, B.M., 2014. What we talk about when we talk about fat. *Cell* 156(1–2):20–44.
- [27] Wang, F., Mullican, S.E., DiSpirito, J.R., Peed, L.C., Lazar, M.A., 2013. Lipotrophy and severe metabolic disturbance in mice with fat-specific deletion of PPARgamma. *Proceedings of the National Academy of Science United States of America* 110(46):18656–18661.
- [28] Gupta, R.K., Mepani, R.J., Kleiner, S., Lo, J.C., Khandekar, M.J., Cohen, P., et al., 2012. Zfp423 expression identifies committed preadipocytes and localizes to adipose endothelial and perivascular cells. *Cell Metabolism* 15(2):230–239.
- [29] Vishvanath, L., MacPherson, K.A., Hepler, C., Wang, Q.A., Shao, M., Spurgin, S.B., et al., 2016. Pdgfrbeta+ mural preadipocytes contribute to adipocyte hyperplasia induced by high-fat-diet feeding and prolonged cold exposure in adult mice. *Cell Metabolism* 23(2):350–359.
- [30] Gupta, R.K., Arany, Z., Seale, P., Mepani, R.J., Ye, L., Conroe, H.M., et al., 2010. Transcriptional control of preadipocyte determination by Zfp423. *Nature* 464(7288):619–623.
- [31] Shao, M., Ishibashi, J., Kusminski, C.M., Wang, Q.A., Hepler, C., Vishvanath, L., et al., 2016. Zfp423 maintains white adipocyte identity through suppression of the beige cell thermogenic gene program. *Cell Metabolism*.
- [32] Alcaraz, W.A., Gold, D.A., Raponi, E., Gent, P.M., Concepcion, D., Hamilton, B.A., 2006. Zfp423 controls proliferation and differentiation of neural precursors in cerebellar vermis formation. *Proceedings of the National Academy of Science United States of America* 103(51):19424–19429.
- [33] Cheng, L.E., Zhang, J., Reed, R.R., 2007. The transcription factor Zfp423/OAZ is required for cerebellar development and CNS midline patterning. *Developmental Biology* 307(1):43–52.
- [34] Warming, S., Rachel, R.A., Jenkins, N.A., Copeland, N.G., 2006. Zfp423 is required for normal cerebellar development. *Molecular and Cell Biology* 26(18):6913–6922.
- [35] Wang, Q.A., Tao, C., Gupta, R.K., Scherer, P.E., 2013. Tracking adipogenesis during white adipose tissue development, expansion and regeneration. *Nature Medicine* 19(10):1338–1344.
- [36] Parlee, S.D., Lentz, S.I., Mori, H., MacDougald, O.A., 2014. Quantifying size and number of adipocytes in adipose tissue. *Methods in Enzymology* 537:93–122.
- [37] Berry, R., Rodeheffer, M.S., 2013. Characterization of the adipocyte cellular lineage in vivo. *Nature Cell Biology* 15(3):302–308.
- [38] Hong, K.Y., Bae, H., Park, I., Park, D.Y., Kim, K.H., Kubota, Y., et al., 2015. Perilipin+ embryonic preadipocytes actively proliferate along growing vasculatures for adipose expansion. *Development* 142(15):2623–2632.
- [39] Unger, R.H., Scherer, P.E., 2010. Gluttony, sloth and the metabolic syndrome: a roadmap to lipotoxicity. *Trends in Endocrinology & Metabolism* 21(6):345–352.
- [40] Jiang, Y., Berry, D.C., Tang, W., Graff, J.M., 2014. Independent stem cell lineages regulate adipose organogenesis and adipose homeostasis. *Cell Reports* 9(3):1007–1022.
- [41] Kang, S., Kong, X., Rosen, E.D., 2014. Adipocyte-specific transgenic and knockout models. *Methods in Enzymology* 537:1–16.
- [42] Senol-Cosar, O., Flach, R.J., DiStefano, M., Chawla, A., Nicoloso, S., Straubhaar, J., et al., 2016. Tenomodulin promotes human adipocyte differentiation and beneficial visceral adipose tissue expansion. *Nature Communications* 7:10686.